Iyer, Ajai; Kaskela, Antti; Novikov, Serguei; Etula, Jarkko; Liu, Xuwen; Kauppinen, Esko I.; Koskinen, Jari

Effect of tetrahedral amorphous carbon coating on the resistivity and wear of single-walled carbon nanotube network

Published in:
Journal of Applied Physics

DOI:
10.1063/1.4948672

Published: 14/05/2016

Document Version
Publisher's PDF, also known as Version of record

Please cite the original version:
Iyer, A., Kaskela, A., Novikov, S., Etula, J., Liu, X., Kauppinen, E. I., & Koskinen, J. (2016). Effect of tetrahedral amorphous carbon coating on the resistivity and wear of single-walled carbon nanotube network. *Journal of Applied Physics*, *119*(18), Article 185306. https://doi.org/10.1063/1.4948672

AIP Journal of Applied Physics

Effect of tetrahedral amorphous carbon coating on the resistivity and wear of single-walled carbon nanotube network

Ajai Iyer, Antti Kaskela, Serguei Novikov, Jarkko Etula, Xuwen Liu, Esko I. Kauppinen, and Jari Koskinen

Citation: Journal of Applied Physics **119**, 185306 (2016); doi: 10.1063/1.4948672
View online: http://dx.doi.org/10.1063/1.4948672
View Table of Contents: http://scitation.aip.org/content/aip/journal/jap/119/18?ver=pdfcov
Published by the AIP Publishing

Effect of tetrahedral amorphous carbon coating on the resistivity and wear of single-walled carbon nanotube network

Ajai Iyer,[1,a)] Antti Kaskela,[2] Serguei Novikov,[3] Jarkko Etula,[1] Xuwen Liu,[1] Esko I. Kauppinen,[2] and Jari Koskinen[1]
[1]*Department of Materials Science and Engineering, School of Chemical Technology, Aalto University, P.O. Box 16200, 00076 Espoo, Finland*
[2]*NanoMaterials Group, Department of Applied Physics, School of Science, Aalto University, P.O. Box 15100, 00076 Espoo, Finland*
[3]*Department of Micro and Nanosciences, Aalto University, P.O. Box 13500, 00076 Aalto, Finland*

(Received 16 February 2016; accepted 23 April 2016; published online 12 May 2016)

Single walled carbon nanotube networks (SWCNTNs) were coated by tetrahedral amorphous carbon (ta-C) to improve the mechanical wear properties of the composite film. The ta-C deposition was performed by using pulsed filtered cathodic vacuum arc method resulting in the generation of C+ ions in the energy range of 40–60 eV which coalesce to form a ta-C film. The primary disadvantage of this process is a significant increase in the electrical resistance of the SWCNTN post coating. The increase in the SWCNTN resistance is attributed primarily to the intrinsic stress of the ta-C coating which affects the inter-bundle junction resistance between the SWCNTN bundles. E-beam evaporated carbon was deposited on the SWCNTNs prior to the ta-C deposition in order to protect the SWCNTN from the intrinsic stress of the ta-C film. The causes of changes in electrical resistance and the effect of evaporated carbon thickness on the changes in electrical resistance and mechanical wear properties have been studied. *Published by AIP Publishing.*
[http://dx.doi.org/10.1063/1.4948672]

I. INTRODUCTION

Single walled carbon nanotubes (SWCNTs) have been extensively researched due to their unique electrical and mechanical properties. There are a variety of applications utilizing the electronic properties of SWCNTs such as field effect transistors,[1,2] composite conductors,[3] field emitters,[3] and sensors,[3] to name a few. Due to the difficulty in fabricating un-bundled SWCNTs and then positioning those accurately, substantial work has been performed in trying to utilize SWCNT networks (SWCNTNs) consisting of bundled SWCNT for various applications. The most common applications of such CNT networks are transparent conductive films,[4,5] bio-sensors,[6] interconnects,[7] and thin film transistors,[8] to name a few. Even though individual SWCNT bundles have extremely good mechanical properties with the breaking strength of 13–52 GPa and Young's modulus of 320–1470 GPa,[9] the SWCNT networks as a whole are quite fragile. The SWCNT networks are formed by randomly oriented SWCNT bundles[10] which are entangled due to purely physical forces (Van der Waals). Since there are no strong bonds, either between individual tubes in a bundle or between bundles, the SWCNT networks are mechanically fragile and even the gentlest of mechanical abrasions could damage the SWCNT network sufficiently to negatively affect its electrical properties. The simplest solution to this problem is to coat the SWCNT networks by a hard protective film having good mechanical properties. Diamond like carbon (DLC) coatings, deposited by energetic means, are mechanically robust and a suitable candidate. Many forms of DLC can be deposited, but the most durable form is tetrahedral amorphous carbon (ta-C) which has exceptional mechanical properties, such as hardness of around 80 GPa, Young's modulus of around 700 GPa, and shear modulus of around 300 GPa.[11] Pulsed laser deposition (PLD) was used to coat SWCNTNs by 50 nm of ta-C with good results.[12]

One aspect observed when ta-C deposition is performed on the SWCNTN is the substantial increase in resistivity of the SWCNT network during the process of ta-C deposition. Schittenhelm *et al.*[12] observed the increase in the resistivity from the first pulses of PLD process, and the final resistance of the SWCNTN is 3 to 10^4 times higher. This loss of conductivity has been attributed to the damage of the SWCNT bundles due to high energy C+ ion bombardment.[12,13] In our previous work,[14] we have shown that the high quality ta-C thin films can be deposited, using the pulsed filtered cathodic vacuum arc (p-FCVA) process on SWCNT networks. It was also observed that the ta-C deposited by the p-FCVA process, with a thickness of 20 nm on the SWCNT network,[14] provides sufficient mechanical protection, although the SWCNTN has an increase in the resistance similar to that observed by Schittenhelm *et al.*[12] However, the SRIM simulations show that the penetration depth for even 100 eV C+ ions in SWCNT networks (density around 1.33 g/cc) is around 1 nm,[12] while the typical ion energies in p-FCVA are around 40–60 eV. Even if the porosity of the SWCNT network is factored in and the damage depth is considered to be more, the loss of conductivity is still dis-proportionately large. Also, it has been shown in the literature that the conductivity of an SWCNT network is dependent more on the inter-bundle junction conductivity[15] than on the conductivity

a)Author to whom correspondence should be addressed. Electronic mail: ajai.iyer@aalto.fi. Tel.: +358504603256.

TABLE I. Sample details for the samples tested in this work. SG in the sample name indicates samples fabricated on silicon and glass both with the same thickness of evaporated carbon coating. Two different ta-C coatings have been applied onto the samples. The total film thickness was measured on silicon substrates post evaporated carbon deposition and 20 nm ta-C/50 nm ta-C deposition, respectively.

Sample name	Substrate type	Evaporated carbon coating (nm)	ta-C coating thickness (nm)	Total film thickness (nm)
Href-SG	Silicon and glass	0	20/50	$62.63 \pm 1.6/75.61 \pm 1.4$
H3-SG	Silicon and glass	3 ± 0.5	20/50	$69.27 \pm 0.22/78.65 \pm 2.5$
H6-SG	Silicon and glass	6 ± 0.6	20/50	$71.31 \pm 4.9/82.30 \pm 0.49$
H9-SG	Silicon and glass	9 ± 0.4	20/50	$73.85 \pm 2.88/88.89 \pm 2.3$

of individual tubes/bundles. Considering these factors, the change in resistivity of the SWCNTN during ta-C deposition observed in Ref. 12 and also by us in the course of the previous work[14] is puzzling.

In this manuscript, a series of SWCNTN samples were investigated to ascertain the dominant reason for increase in the SWCNTN resistivity, when ta-C is deposited on them. The SWCNTNs were coated with different thicknesses of low energy evaporated carbon film prior to the ta-C deposition. Evaporation of carbon was done by using an e-beam system, and the evaporated coating on the SWCNTNs was expected to act as a protective thin film against carbon ion bombardment. Pulsed filtered cathodic vacuum Arc (p-FCVA) process was used to deposit ta-C on the samples, and the electrical resistance was measured in-situ. The samples were characterized by profilometry, scanning electron microscope (SEM), transmission electron microscope (TEM), atomic force microscopy (AFM), Raman spectroscopy, and UV-Vis spectrophotometry. Nano-wear tests were performed with different applied loads to investigate the wear protection offered by ta-C coating and the effect of underlying evaporated carbon layer on the mechanical properties of the composite film.

II. EXPERIMENTAL DETAILS

SWCNTs were synthesized by high temperature floating catalyst CVD process by thermal decomposition of ferrocene as explained in detail elsewhere.[4,14] The SWCNTs formed aggregate in gas phase to form bundles due to surface energy minimization[10] and were collected on nitrocellulose membranes (Millipore Ltd. HAWP, 0.45 μm pore size) at the outlet of the reactor. SWCNTs collected on the membrane form randomly oriented SWCNTNs which can be transferred onto other substrates.

Silicon (100) with resistance more than 1000 Ω cm and the glass (Metzeler) cut into 3 cm × 2 cm pieces were used as substrates. The substrates were cleaned by sonication for 3 minutes in High performance liquid chromatography grade acetone, blow dried by nitrogen, and put on a hot plate at 120 °C for a few minutes to remove any adsorbed water. The SWCNTNs were transferred onto the substrates using a room temperature press transfer process explained in detail elsewhere.[4,14] The membrane filters with the SWCNT film on them were cut into strips around 2 cm × 1.5 cm and placed SWCNTN side down on the substrates and pressed between the clean glass slides with a pressure of around 10^5 Pa.[4,14] The membrane filter backing was peeled off carefully, leaving the SWCNTN adhered to the substrate surface. Following this, the SWCNTN was densified by the addition of few drops of ethanol to the film.[4,14] The samples were dried on a hot plate at 120 °C for 3 min to remove any adsorbed water. Contact pads, for 2 point resistivity measurements, were fabricated for all samples at the two ends of the press transferred SWCNTNs by silver conductive paint (Electrolube). The silver contact pads were allowed to dry at room temperature for around 10 min and then dried on a hot plate at 60 °C for few minutes to evaporate all the solvents. Silver paint was chosen, as it allows the formation of substrate insensitive, durable contact pads on the SWCNTN by a low energy and low temperature process in comparison to the sputtered metal contacts, which lead to the SWCNTN damage and are easily de-laminated, as found from pre-tests. Table I shows the samples under test and the resistance values of the SWCNTN samples under different conditions are listed in Table II.

Different thicknesses of evaporated carbon were deposited onto the samples using an e-beam evaporation system (Varian) to compare the effect of protection as a function of evaporated carbon thickness. The e-beam evaporation was performed under high vacuum conditions (vacuum better than 2×10^{-6} Torr). Electrons were generated by tungsten filament (filament current around 100 mA) and accelerated by high voltage (around 4 kV), and the electron beam was directed into a water cooled crucible with 99.999% pure graphite pieces. The deposition was started when the stable evaporation rate of around 1.5–2 Å/s was achieved and the

TABLE II. Resistance values for different samples under test.

Sample name	Resistance in ambient pre-coating (kΩ)	E-beam evaporated carbon coating thickness (nm)	Resistance in ambient post E-beam coating (kΩ)	Stable vacuum resistance ($R_{initial\_Vac}$) (kΩ)
Href-SG	0.227	0	0.227	0.585
H3-SG	0.155	3 ± 0.5	0.598	1.290
H6-SG	0.126	6 ± 0.6	1.061	2.206
H9-SG	0.150	9 ± 0.4	0.555	1.016

deposition thickness was measured by using a crystal thickness monitor (Infinicon). Three different thicknesses of evaporated carbon were deposited on samples, namely, 3 ± 0.5 nm, 6 ± 0.6 nm, and 9 ± 0.4 nm (see Table I). During deposition, the edge of the substrate and half the silver contact pad was masked to avoid carbon deposition over the edges. Pre-tests with silver pads painted on glass substrates with no SWCNTN and 12 nm of e-beam carbon film show that the carbon film has high resistance values of around 600 kΩ as confirmed by the literature.[16] Hence, the carbon coating on the SWCNTN and on the substrate between the exposed silver contacts does not contribute significantly to the resistance of the final sample.

Pulsed filtered cathodic vacuum arc (p-FCVA) process was used to deposit ta-C on the samples. Graphite rods with a diameter of 6.35 mm and 99.95% purity (Graphitestore) were used in a dual cathode system, coupled to a knee filter (45° bend) to filter out macro-particles and guide the plasma.[17] A pulse forming network (PFN), charged to −400 V (pulse current 650 A), was used to strike triggerless arc[18] between cathode and anode body resulting in the formation of carbon plasma. The plasma consists of C+ ions with ion energy between 40 and 60 eV.[19] The PFN was controlled by a custom made National Instruments hardware and LabView software allowing the control of a pulse frequency (set to 1 Hz) and a number of pulses. Depositions were performed at the room temperature with a target to substrate distance of 110 mm. The samples were at the floating potential and were rotated at 20 rpm to ensure the homogeneous deposition of ta-C. The process parameters for the ta-C deposition on samples have been taken from our previous work[14] where it has been shown that the high quality ta-C can be deposited on the SWCNTN by the p-FCVA deposition process. The deposition rate of ta-C was found to be around 0.1 nm/pulse for target to substrate distance of 110 mm measured by using contact profilometer Dektak 6 M (Vecco). Two different ta-C thicknesses were deposited on samples, namely, 50 nm and 20 nm to evaluate the differences in the sample resistance and wear.

In situ measurement of the resistance was performed using a digital multi-meter (HP34401A) which was connected to the contact pads of the substrate via vacuum feedthrough. The sample was kept in the chamber under high vacuum (better than 2×10^{-7} Torr) overnight to desorb gases and attain stable resistance values ($R_{initial\_Vac}$) as shown in Table II. The increase in the resistivity of samples was monitored by depositing maximum thickness of ta-C required, namely, 50 nm (equivalent 500 pulses). For the first 20 pulses, the resistance of the sample was recorded per pulse; subsequently, the resistance of the sample was recorded at intervals of 20 pulses till the completion of 200 pulses. Following this, the resistance of the sample was noted every 100 pulses till the end of deposition (500 pulses). In all cases, prior to recording the resistance value, a settling time of 30 s was allowed to let the resistance value stabilize. For resistance measurements, glass substrate samples were preferred and the rotation was disabled due to fixed connection of multi-meter leads, although silicon substrate samples were also checked and showed a similar behaviour.

Samples fabricated in this work were analysed by scanning electron microscope (SEM) S-4700 (Hitachi) at different stages of the process. SWCNTN areal coverage, defined as the fraction of substrate area covered by the SWCNTN, was ascertained by image analysis of multiple SEM images using ImageJ software. Atomic force microscopy (AFM) using Dimension-5000 (Vecco) system, operated in a tapping mode, was used to evaluate the morphology of pristine SWCNTN. Contact profilometry using Dektak 6 M (Vecco) was performed to ascertain the film thicknesses of the samples.

Raman spectroscopy was performed on the samples by using LabRAM HR (Jobin Yvon Horiba) confocal Raman system. Argon laser (wavelength = 488 nm, power = 10 mW) with a BX41 (Olympus) microscope and 100× objective with a spot size less than 1 μm were used for all samples. All the Raman spectra plots shown in this manuscript are self-normalized with respect to the silicon peak. Optical properties of samples at different stages of process were checked by Lambda 950 (Perkin Elmer) UV-Vis spectrophotometer. For all the samples, a metallic beam stopper with a 3 mm diameter hole was used, to ensure known and controllable area of measurement around the center of sample.

Transmission electron microscopy (TEM) was performed on the samples using Tecnai F-20 (FEI) TEM operating at 200 kV. Pristine SWCNTNs as well as e-beam and ta-C coated samples were scratch transferred onto a 400 mesh copper grid with a holey carbon film (Agar) for TEM analysis.

Nano-mechanical wear testing was performed by TI-900 TriboIndenter (Hysitron Inc) using a Berkowitz tip (nominal diameter 200 nm). Nano-wear tests were performed by scanning four points per sample, in a load controlled mode, with loads from 30 μN to 60 μN with a load increment of 10 μN per point. Scan area for each wear scan was 2 μm × 2 μm and two scan passes were made. Post scan, an area of 6 μm × 6 μm, was imaged using a lower load of 1 μN to avoid any changes in the morphology of the wear scan. Post scan images were processed using Gwyddion image processing software to estimate average wear crater depth and average wear crater area. The wear crater volume was calculated as a product of average crater depth and average crater area for any particular wear scan. The wear volume ratio for samples was calculated as the ratio of crater wear volume to the maximum possible wear volume, where the maximum wear volume corresponds to the product of the film thickness and the wear scan area (4 μm^2).

III. RESULTS AND DISCUSSION

A. Pristine press transferred SWCNTN

Press transferred SWCNTN on silicon substrates was imaged by SEM, and a typical image is shown in Fig. 1(a). Image analysis was performed on multiple images taken from random spots on the samples and the areal coverage of the SWCNTN was estimated to be 70%–75% of the substrate area for all samples. The uncoated SWCNTN were also imaged by TEM (Fig. 1(b)) and bundle diameters were

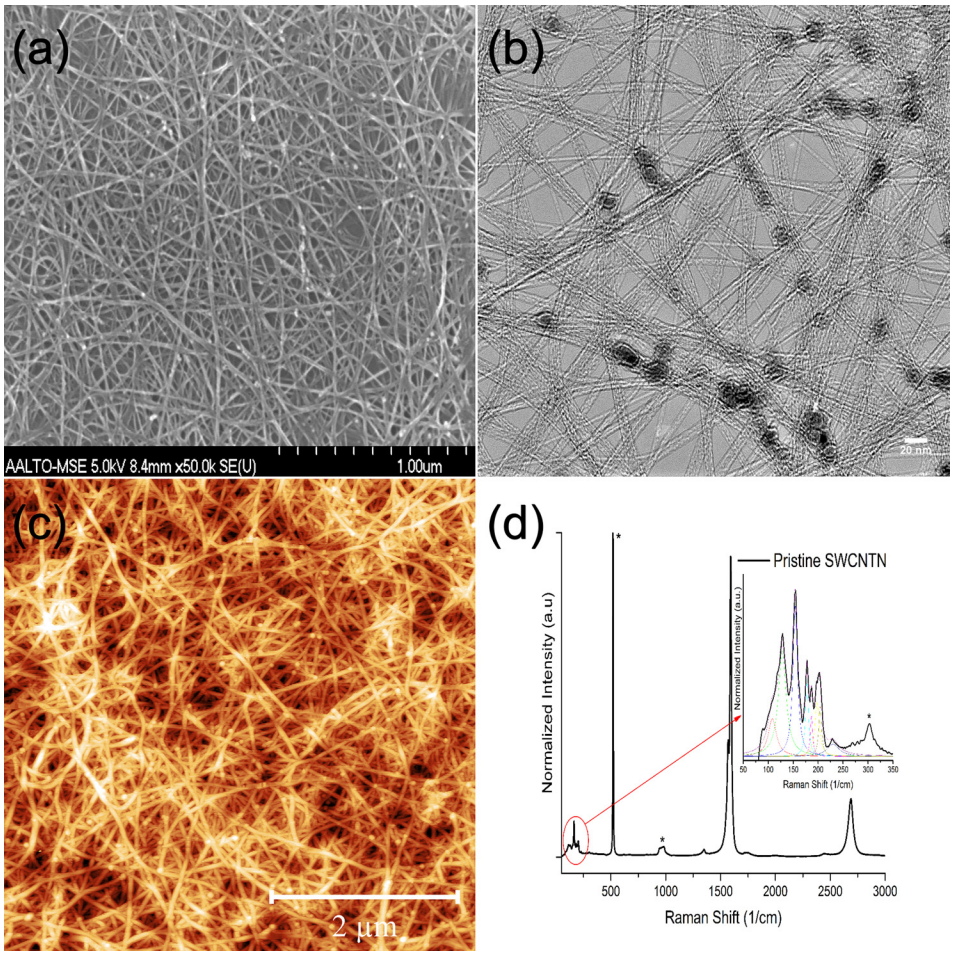

FIG. 1. (a) SEM image of pristine press transferred SWCNTN; (b) TEM micrograph of SWCNTN for bundle thickness estimation; (c) AFM image of the SWCNTN on silicon showing morphology and roughness; and (d) normalized Raman spectra of press transferred SWCNTN on silicon. Inset shows RBM peak fits. * indicates peaks due to Silicon substrate.

observed to be in the range of 3–20 nm. The black particles observed in the TEM image (Fig. 1(b)) were identified as iron nanoparticles from the aerosol growth process of the SWCNTs. The film thickness of press transferred SWCNTN (on silicon substrates) was estimated to be around 45 nm. The AFM imaging of the pristine press transferred SWCNTN (Fig. 1(c)) showed the roughness (Ra) to be around 5 nm.

The Raman spectrum of pristine press transferred SWCNTN self-normalized to silicon peak is shown in Fig. 1(d). From the Raman spectra, radial breathing mode (RBM) peaks were fit using Lorentzians (Fig. 1(d) inset), and using Equation (1),[20] SWCNT diameters were calculated to be in the range of 1–2 nm

$$\omega_{RBM} = \left(\frac{A}{d_t}\right) + B, \tag{1}$$

where $A = 234$ nm/cm and $B = 10\,cm^{-1}$.

B. Evaporated carbon coated samples

The SEM images of samples (on silicon substrate), post e-beam evaporated carbon deposition, were acquired and typical images are shown in Fig. 2. Comparing the images from Figs. 2 and 1(a), it was noted that evaporated carbon coated SWCNTN bundles appear thicker than the pristine bundles (Fig. 1(a)). Increasing bundle thickness and reduction of open areas in the SWCNTN mesh due to the deposition of carbon film were observed as the evaporated carbon coating thickness increases from H3-SG (Fig. 2(a)) to H9-SG (Fig. 2(c)).

Raman spectroscopy was performed on the SWCNTN samples (on silicon substrates) with an evaporated carbon coating (Fig. 3(a)) and on reference 12 nm evaporated carbon coating only (not shown). In case of reference evaporated carbon coating, a broad peak between 1200 and 1600 cm^{-1}, characteristic of amorphous carbon[21,22] was observed. From the Raman spectra of evaporated carbon coated SWCNTN samples, it was observed that the intensity of RBM and G peaks was reduced in comparison to the uncoated SWCNTN, while the D peak intensity was increased. It was also observed that the D and G peaks for the evaporated carbon coated SWCNTN samples "ride" on the signal for amorphous evaporated carbon, especially in case of the thicker film of 9 nm as seen from the Raman plot for H9-SG (Fig. 3(a)). The increase in the D peak intensity observed in case of evaporated carbon coated samples could be attributed to the presence of amorphous carbon layer which has a behaviour similar to the carbonaceous impurities as shown in the literature.[23] The intensity of RBM and G peak also reduces in comparison to the pristine sample due to the evaporated carbon film as shown in the literature.[23] From the SEM images and TEM micrographs (see supplementary Fig. S1[24]), it was observed that the evaporated carbon film forms a coating on the SWCNTN.

UV-Vis spectrophotometry was performed on the SWCNTN samples (on glass substrates) to compare the

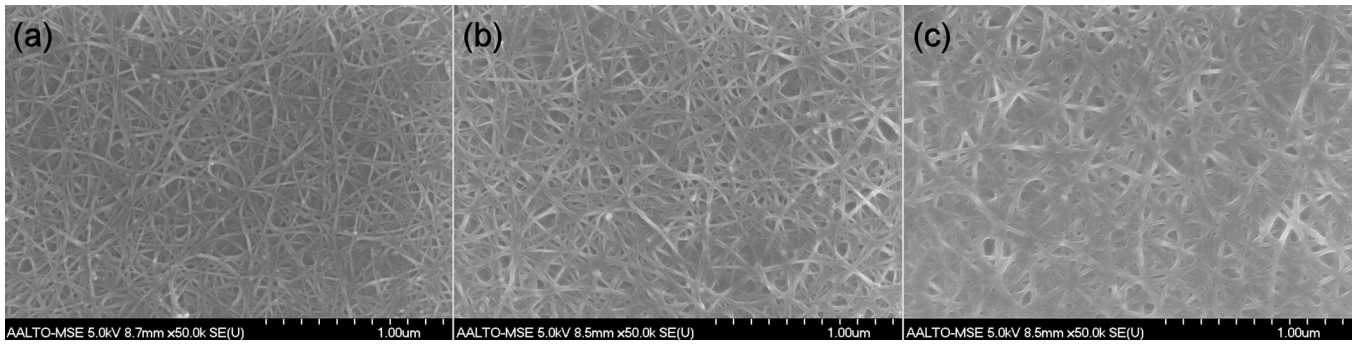

FIG. 2. SEM images of e-beam evaporated carbon coated samples. (a) H3-SG with 3 nm of evaporated carbon coating; (b) H6-SG with 6 nm of evaporated carbon coating; and (c) H9-SG with 9 nm of evaporated carbon coating.

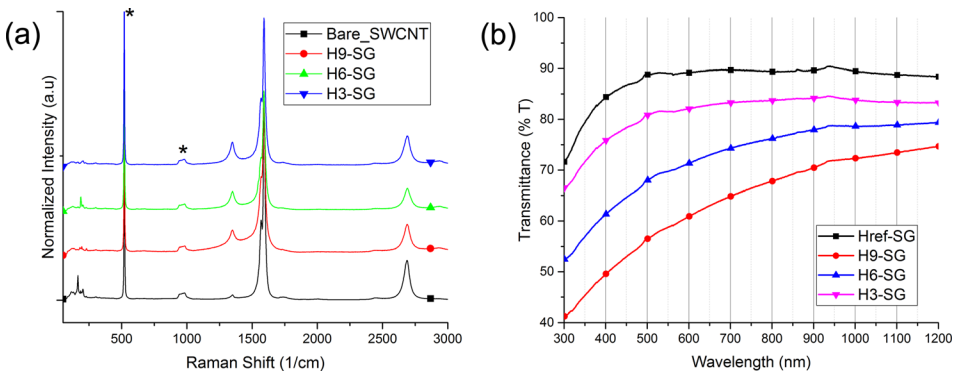

FIG. 3. (a) Raman spectra of pristine SWCNTN and evaporated carbon deposited SWCNTN samples. Traces offset for clarity. * indicates peaks due to silicon substrate and (b) UV-Vis spectrophotometry data comparing the transparency of uncoated SWCNTN (Href-SG) and evaporated carbon coated samples. Note that for both images symbols are for identification of plots only.

transmittance with (H3-SG, H6-SG, and H9-SG) and without (Href-SG) evaporated carbon coating on the SWCNTN (Fig. 3(b)). The average transmittance in the visible region (400 nm–700 nm) was found to be around 88% for Href-SG, 81% for H3-SG, 70% for H6-SG, and 58% for H9-SG. Thus, as per expectation, thinner coating of evaporated carbon had minimal effect on the transmittance of SWCNTN in comparison with the reference sample.

C. Samples coated by ta-C

Typical SEM images of 20 nm ta-C deposited on samples are shown in Fig. 4. The SEM images of 50 nm ta-C deposited on samples were found to have greatly increased the bundle thickness and almost no visible clear areas in the SWCNTN mesh structure (see supplementary Fig. S2[24]). The difference in morphology between the pristine samples

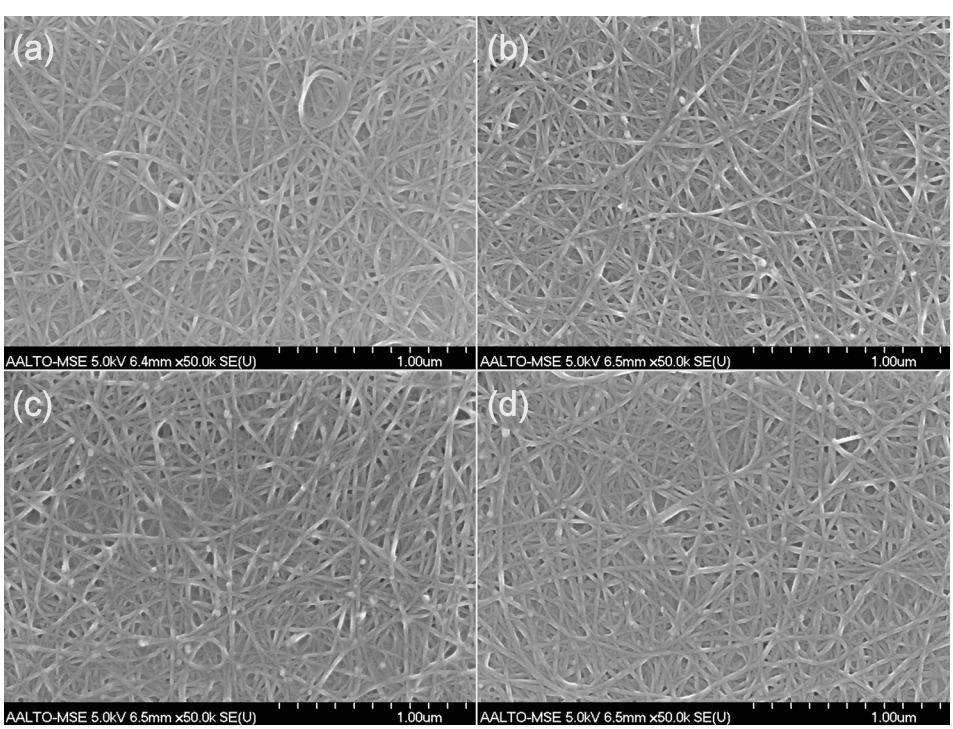

FIG. 4. SEM images of 20 nm ta-C coated samples. (a) Href-SG; (b) H3-SG with 3 nm of evaporated carbon coating pre ta-C; (c) H6-SG with 6 nm of evaporated carbon coating pre ta-C; and (d) H9-SG with 9 nm of evaporated carbon coating pre ta-C.

(Fig. 1(a)) and evaporated carbon coated samples (Fig. 2) is clearly seen. Raman spectra from the ta-C coated parts of the samples, not covered by the SWCNTN, were plotted (see supplementary Fig. S3[24]). Raman plots for ta-C were fit by Gaussians for the D and G regions[11,22] with resulting I(D)/I(G) ratios in the range of 0.2 (Href-SG) to 0.4 (H9-SG). Changes in the resistivity of samples when ta-C is deposited were tested *in-situ*, by depositing the maximum thickness (50 nm) of ta-C (see Sec. II). The resistivity test data discussed here are from the samples on glass substrates, although the samples on silicon substrates were also tested, and the results are similar in all respect. Samples under test were kept in high vacuum conditions till stable resistance values were achieved (see Sec. II) which corresponds to the initial resistance value of the sample ($R_{initial\_Vac}$) as shown in Table II. The SWCNTN has a significant increase in resistance under vacuum conditions compared to ambient due to the desorption of molecules from the SWCNTN.[25,26] Increase in resistance as a function of ta-C pulses was measured (R_{point}) and Fig. 5 plots the rate of increase (ROI) of resistance for different samples against the number of ta-C pulses, where the ROI was calculated using the following equation:

$$\mathrm{ROI}\,(\%) = ((R_{initial\_Vac} - R_{point})/R_{initial\_Vac}) * 100. \quad (2)$$

Note that the plot in Fig. 5 is a semi-log plot with ROI of resistance plotted in log scale.

From Fig. 5, the ROI of resistance at the end of the test (500 pulses or 50 nm ta-C) is around 4500% for Href-SG, 166% for H3-SG, 141% for H6-SG, and 91% for H9-SG. The ROI of resistance even for sample H3-SG with minimum evaporated carbon coating is phenomenally lower than for the reference sample (Href-SG). It was also noted from Fig. 5 that in all cases, the maximum ROI of resistance occurs for the first few ta-C pulses and subsequently reduces or stabilizes around 40–60 pulses (equivalent 4–6 nm ta-C). The increase in resistance due to deposition of ta-C may be attributed to two main factors, which are discussed below. One factor is the C+ ion bombardment, which has been shown experimentally[13] and by simulation[27] methods to damage SWCNTs. However, the ion energies in the p-FCVA process (40–60 eV) are sufficient for penetration of at most 1–2 nm of the SWCNTN[12] and the evaporated carbon coated samples should be immune to the C+ ion bombardment damage. Even if variations in the thickness of evaporated carbon are factored in, then even in the worst case there should be no observable increase of resistance with ta-C deposition for samples H6-SG and H9-SG due to the protection of evaporated carbon coating, which is contrary to the observations made (Fig. 5). The other factor which must be considered is the stress induced during the process of ta-C film formation. The formation of ta-C film from energetic ions has been explained by the sub-plantation model[28–30] wherein the C+ ion penetrates a few angstrom below the substrate surface, and due to the increase in pressure/density, sp^3 bond formation is promoted.[28–30] This sub-plantation process continues throughout the period of ta-C film deposition leading to compressive stress in the ta-C films in the range of 2–8 GPa[11,30] and a few angstrom thick sp^2 layer at the very top when deposition process is terminated.[11,28–30] It has also been shown that the resistivity of SWCNT bundles changes when subjected to pressure and there is a sharp increase in the resistivity with the increase in pressure.[31] Thus, a working hypothesis could be formed that the evolving stress in the ta-C film is responsible for the changes in the resistance of the SWCNTN.

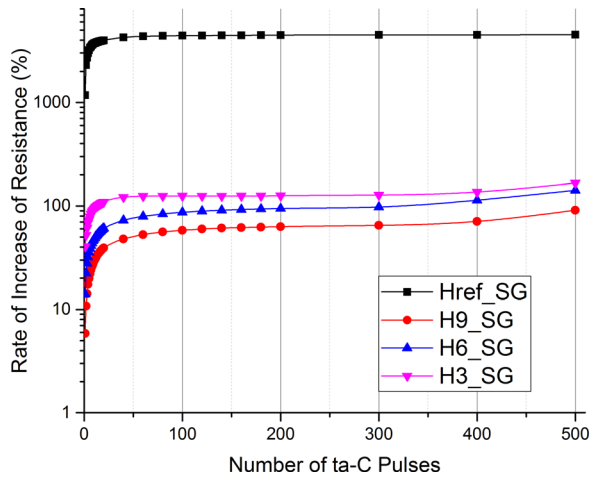

FIG. 5. Semi-log plot showing the Rate of Increase of Resistance (in %) for the samples as a function of number of ta-C pulses deposited on them.

The effects of stress on the Raman spectra of SWNTs are profound and shown in the literature.[32–34] The Raman spectra of samples (on silicon substrates) post deposition of 20 nm and 50 nm of ta-C were acquired and are shown in Figs. 6(a) and 6(b), respectively. Comparing the Raman spectra of ta-C coated SWCNTN samples (Figs. 6(a) and 6(b)) to the pristine uncoated SWCNTN, it was observed that the RBM peaks are greatly suppressed, while the G peak had reduced in intensity and broadened. However, the D peak intensity had not increased, as it should increase in case of heavy damage due to ion bombardment.[13] It was also observed that the D and G peaks "ride" on the signal for ta-C (see supplementary Figs. S3 and S4[24]), and is most evident in case of 50 nm ta-C coating (Fig. 6(b)) as shown previously in the literature.[12,14] However, no shift in D or G peak position was observed in the acquired Raman spectra (Fig. 6) as is expected in case of SWCNT bundles under stress.[32–34] This indicates that the SWCNTs forming the network are not under stress post deposition of ta-C.

Although the Raman spectra indicate that the SWCNTN is not under stress, this does not invalidate our hypotheses of the stress in ta-C changing the resistance of networks. The resistance of SWCNTN has been shown to be dominated by the resistance of the junctions.[15,35] It has also been shown by mechanical tests coupled with *in situ* Raman analysis that when the SWCNT bundles are mechanically stressed, they tend to relax the stress, either by changing their physical morphology (by bending or twisting) or by the slippage or sliding of tubes in the bundle.[36,37] Such processes do not introduce any deformations to the SWCNTs which could be monitored by Raman spectroscopy.[36,37] In the case of our samples, the compressive stress due to ta-C would be transmitted to the substrate (SWCNTNs with or without

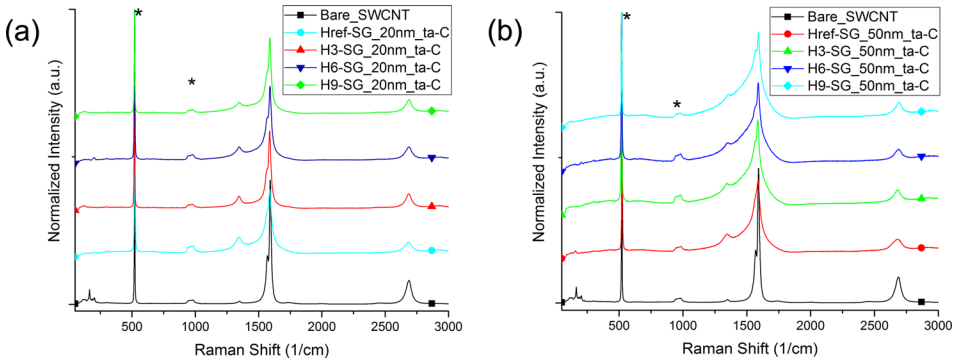

FIG. 6. Raman spectra of samples post ta-C deposition. (a) Comparison of Raman spectra for pristine uncoated SWCNTN and 20 nm ta-C coated SWCNTN and (b) comparison of Raman spectra for pristine uncoated SWCNTN and 50 nm ta-C coated SWCNTN. For both plots, Raman spectra of samples have been offset and marked by the symbols for visibility and * indicates peaks due to silicon.

evaporated carbon coating) where the SWCNTs in the bundles would try to relieve the stress either by changing their physical morphology or by the slipping of individual SWCNTs from the bundle. This would result in significant changes to the SWCNT junction contacts either due to increased junction contact separation (changes in physical morphology) or by changing of the junction contact point (slippage of tubes in a bundle) or both. Any changes to the SWCNT junction contact resistance due to the above process would be global over the whole sample area, as ta-C coating is global over the whole sample area. This increase in junction resistance over the whole sample area would have a significant effect on the overall resistance as is seen from Fig. 5, but no shift of D or G peak would be observed in the Raman spectra (Fig. 6). The slippage of SWCNT tubes from bundles was also observed in TEM images (see supplementary Fig. S1[24]) of 50 nm ta-C flake which has SWCNTs dangling from the edges similar to the observations by Ajayan *et al.*[36]

Thus, in case of Href-SG with no evaporated carbon film, the increase in the resistance could be attributed to ion bombardment damage initially, followed by the intrinsic stress due to the ta-C film changing the junction resistance. Even after the formation of a few nanometers thick ta-C film, which would protect the underlying SWCNTN from ion bombardment, the resistance continues to increase due to the increasing stress of the ta-C film, as can be seen from Fig. 5. In case of the evaporated carbon coated samples (H3-SG to H9-SG), the ta-C formation would start from within the evaporated carbon film and not from the SWCNTN, according to the sub-plantation model[28–30] and the SWCNTN would be protected from the C+ ion bombardment damage. Also, it has been shown that multilayer coatings composed of alternate soft and hard carbon thin films reduce the overall stress of the complete multilayer coating.[38,39] Thus in the case of evaporated carbon coated samples, the stress of the growing ta-C film could be less due to a relatively softer evaporated carbon layer below hard ta-C coating (see supplementary Raman discussion[24]). Also, to the best understanding of the authors, the softer evaporated carbon layer would reduce the transmission of stress from the growing ta-C film to the SWCNTN, dependent on the thickness of the evaporated carbon film. These effects were observed in Fig. 5, where the thickest evaporated carbon film (H9-SG) has the smallest ROI of resistance compared to the other samples and all the evaporated carbon samples perform significantly better than the reference sample (Href-SG). For samples with evaporated carbon (H3-SG to H9-SG), a small increase in the ROI of resistance in the latter part of the test (300 pulses and above in Fig. 5) was observed, which could be due to the relatively softer evaporated carbon film transmitting more stress to the SWCNTN with increasing thickness (and thus increasing stress) of ta-C film.[40]

From the above discussion, the theory formed indicates that the dominant reason for increase of resistance for the SWCNTN when coated by ta-C is due to the changes in junction resistance caused by the movement of SWCNT tubes/bundles. Logically, etching some ta-C away should reduce the stress of the film, due to the reduction of thickness and some of the junctions (if not all) should relax, re-establishing old contacts and reducing the resistance. Sample Href-SG with 50 nm of ta-C was subjected to mild oxygen plasma etching by Fischione Instruments Model 1020 plasma cleaner (75% Argon + 25% Oxygen, 12–15 eV ion energy). Such a plasma etch is suitable to etch ta-C as shown in the literature[14,41] and etch rates found by calibration were around 0.125 nm/s. The etching was performed for 3 min (etch thickness around 22 nm) and the sample was put back in vacuum to check the resistance. Compared to the final vacuum resistance value, post deposition of 50 nm of ta-C, etched sample Href-SG showed around 30% reduction in resistance. Raman spectra were acquired from the sample post oxygen plasma etching and comparison with pre-etch spectra (Fig. 7(a)) revealed no shift in D or G peak positions, although post etching RBM peaks are more prominent. This seems to indicate that the theory formulated is valid and further tests are in progress on the other samples.

UV-Vis spectroscopy was performed after deposition of 20 nm ta-C on samples and the plot shown in Fig. 7(b). The average transmittance calculated between 400 nm and 700 nm for samples were 71% for Href-SG, 66% for H3-SG, 63% for H6-SG, and 57% for H9-SG. Although these transmittance values are low, some of the decrease is due to the ta-C itself (due to sp^2 content) which had an average transmittance of 81% in the same region. It would be possible to improve the transparency of the samples by performing cycles of mild oxygen plasma treatment to etch some of the ta-C off with most of the sp^2 top layers[11,28–30] and then deposit ta-C again as shown by Dwivedi *et al.*[41]

It had been shown in our previous work[14] that even 20 nm thick ta-C films on SWCNTN provide adequate wear protection in comparison to the un-coated SWCNTN.

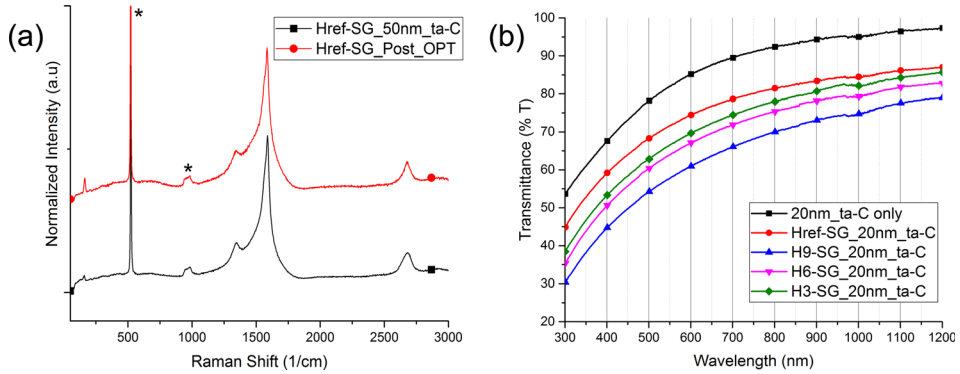

FIG. 7. (a) Comparison of Raman spectra of pre- and post-oxygen plasma etching of the sample. Href-SG_50 nm_ta-C is the Raman spectra of the 50 nm ta-C coated SWCNT sample, pre-oxygen plasma etching, while Href-SG_Post_OPT is the Raman spectra of the same sample post 3 min of oxygen plasma etching. For both plots, Raman spectra of samples have been offset for clarity and * indicates peaks due to silicon; (b) UV-Vis spectrophotometry data of 20 nm ta-C coated samples. Please note that for both images symbols are for identification of plots only.

Nano-wear testing was performed on silicon substrate samples to ascertain the effect of evaporated carbon coating on the wear properties of ta-C coated samples. Tests performed (not shown) with the uncoated SWCNTN samples resulted in the removal of SWCNTN on the silicon substrate even for smallest test force of 30 μN. Results of tests performed (not shown) on the SWCNTN samples with different thicknesses of evaporated carbon coating were similar to the uncoated SWCNTN samples, indicating that the evaporated carbon coating had none or minimal wear protection. Plots of wear ratio against the applied load are shown in Fig. 8(a) for 20 nm ta-C coated samples and in Fig. 8(b) for 50 nm ta-C coated samples. Comparing the plots for 20 nm and 50 nm ta-C coated samples (Figs. 8(a) and 8(b)), it was observed that the maximum wear ratio is around 7.5% for 50 nm samples and around 60% for 20 nm ta-C coated samples. Thus, it can be inferred that 50 nm ta-C coated samples were more wear resistant than 20 nm ta-C coated samples and the increase in resistance is not phenomenal (Fig. 5) to avoid thicker coating. Furthermore, detailed study of wear plots and correlation with I(D)/I(G) ratios (see supplementary Raman discussion[24]) revealed interesting trends. In case of 20 nm ta-C coated sample (Fig. 8(a)) comparing wear ratios, it was observed that sample H3-SG performs worse than reference (Href-SG), while H6-SG performs slightly better than reference and H9-SG performs best. To the best understanding of the authors, the wear performance of samples was dependent on the thickness of evaporated carbon films underlying the ta-C, as explained below. As has been stated previously, the ta-C formation is due to the sub-plantation process of energetic C+ ions. In case of H3-SG, the evaporated carbon film (3 nm) and variation in its thickness do not allow for stable interface formation during ta-C deposition,[33] as a result of which the composite had higher wear due to improper adhesion. However, H6-SG and H9-SG had a thicker evaporated carbon film leading to stable interface and good adhesion. In addition, in case of H9-SG, the increased thickness of evaporated carbon film coupled to the SWCNTN provides a visco-elastic medium below the hard ta-C coating. Hence, with increase of applied load, the visco-elastic medium below ta-C deforms and then partially recovers on removal of the load, leading to an overall reduction of wear. The trend for 50 nm ta-C film (Fig. 8(b)) was different, as the ta-C film behaves as bulk now (as inferred from I(D)/I(G) ratios supplementary Table I[24]), and wear ratio of all samples is low. Also, all the evaporated carbon coated samples wear lower than reference (Href-SG) with H9-SG having lowest wear for the reasons explained above. In case of 60 μN load point for sample H6-SG with 50 nm ta-C film, the wear ratio is highest as the sample has suffered catastrophic de-lamination during testing (not shown here) due to unknown reasons and the point could be dis-regarded from the trend.

IV. CONCLUSIONS

In this work, three part composite films consisting of SWCNTN, e-beam evaporated carbon, and p-FCVA deposited ta-C were fabricated and characterized.

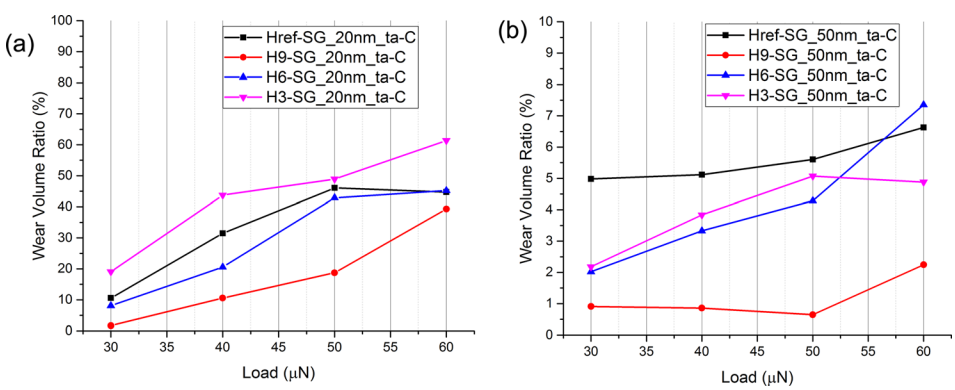

FIG. 8. Wear volume ratio from nano-wear tests. Ratio of crater wear volume to the maximum wear volume of composite film against applied load: (a) for 20 nm thick ta-C films and (b) for 50 nm thick ta-C films.

Results indicate that the dominant reason for increase in the resistance of the SWCNT networks during ta-C deposition could be attributed to the intrinsic compressive stress of the ta-C. The SWCNT bundles relieve the stress imposed on them by the ta-C film by either changing their physical morphology (bending or twisting) or by slippage of the individual tubes from bundles or both. As a part of this stress relief process, the junctions between SWCNT tubes/bundles are affected leading to the increase in the junction resistance over the whole area of the SWCNTN film. In addition, such physical processes of stress relief do not induce any changes in the SWCNT bundles which could be monitored by Raman spectroscopy. Deposition of a protective layer, such as e-beam evaporated carbon, on the SWCNT networks prior to ta-C deposition provides significant reduction of resistance (increase of 4500% in case of no protective coating Href-SG compared to the increase of 91% with 9 nm of evaporated carbon H9-SG). The protective layer serves the dual purpose of protecting against ion induced damage and also dissipating and/or reducing the intrinsic stress of the ta-C film, thus reducing the effect of stress on the resistance of the SWCNT network. Nano-wear testing indicates that a thicker ta-C film provides better wear protection compared to a thinner ta-C film. Also, nano-wear tests indicate that composites with thicker evaporated carbon film have better wear protection irrespective of the thickness of ta-C film.

Thus, it was concluded that coating SWCNT networks with soft, low energy coatings prior to the deposition of hard coating with intrinsic stress would preserve the conductivity of the SWCNT networks to a large extent and enhance the mechanical properties of the coated SWCNT networks.

ACKNOWLEDGMENTS

Sponsorship of Academy of Finland funding via research project HISCON (No. 259595) is acknowledged.

Antti Kaskela and Esko I. Kauppinen also acknowledge the financial support from TEKES via CARLA project, Aalto Energy Efficiency (AEF) program via MOPPI-project and JST-EC DG RTD Co-ordinated research project "IRENA" within the Strategic International Collaborative Research Program (SICORP).

Help given by Mr. Kaustuv Banerjee for AFM imaging is gratefully acknowledged. Aalto University Nanomicroscopy Center (Aalto-NMC) is acknowledged.

[1]S. J. Tans, A. R. M. Verschueren, and C. Dekker, "Room-temperature transistor based on a single carbon nanotube," Nature **393**, 49 (1998).
[2]A. Javey, J. Guo, Q. Wang, M. Lundstrom, and H. Dai, "Ballistic carbon nanotube field-effect transistor," Nature **424**, 654 (2003).
[3]R. H. Baughman, A. A. Zakhidov, and W. A. de Heer, "Carbon nanotubes—The route toward applications," Science **297**, 787 (2002).
[4]A. Kaskela, A. G. Nasibulin, M. Y. Timmermans, B. Aitchison, A. Papadimitratos, Y. Tian, Z. Zhu, H. Jiang, D. P. Brown, A. Zakhidov, and E. I. Kauppinen, "Aerosol synthesized SWCNT networks with tunable conductivity and transparency by a dry transfer technique," Nano Lett. **10**, 4349 (2010).
[5]J. L. Blackburn, T. M. Barnes, M. C. Beard, Y.-H. Kim, R. C. Tenet, T. J. McDonald, B. To, T. J. Coutts, and M. J. Heben, "Transparent conductive single-walled carbon nanotube networks with precisely tunable ratios of semiconducting and metallic nanotubes," ACS Nano **2**, 1266 (2008).
[6]J. Wang, "Carbon-nanotube based electrochemical biosensors: A review," Electroanalysis **17**, 7 (2005).
[7]F. Kreupl, A. P. Graham, G. S. Duesberg, W. Steinhögl, M. Liebau, E. Unger, and W. Hönlain, "Carbon nanotubes in interconnect applications," Microelectron. Eng. **64**, 399 (2002).
[8]D. M. Sun, M. Y. Timmermans, A. Kaskela, A. G. Nasibulin, S. Kishimoto, T. Mizutani, E. I. Kauppinen, and Y. Ohno, "Mouldable all-carbon integrated circuits," Nat. Commun. **4**, 2302 (2013).
[9]M.-F. Yu, B. S. Files, S. Arepalli, and R. S. Ruoff, "Tensile loading of ropes of single wall carbon nanotubes and their mechanical properties," Phys. Rev. Lett. **84**, 5552 (2000).
[10]D. Gonzalez, A. G. Nasibulin, S. D. Shandakov, P. Queipo, H. Jiang, and E. I. Kauppinen, "Single-walled carbon nanotube charging during bundling process in gas phase," Phys. Status Solidi B **243**, 3234 (2006).
[11]J. Robertson, "Diamond like amorphous carbon," Mater. Sci. Eng., R **37**, 129 (2002).
[12]H. Schittenhelm, D. B. Geohegan, G. E. Jellison, A. A. Puretzky, M. J. Lance, and P. F. Britt, "Synthesis and characterization of single-wall carbon nanotube-amorphous diamond thin-film composites," Appl. Phys. Lett. **81**, 2097 (2002).
[13]G. D. Saraiva, A. G. S. Filho, G. Braunstein, E. B. Barros, J. M. Filho, E. C. Moreira, S. B. Fagan, D. L. Bapista, Y. A. Kim, H. Muramatsu, M. Endo, and M. S. Dresselhaus, "Resonance Raman spectroscopy in Si and C ion-implanted double-wall carbon nanotubes," Phys. Rev. B **80**, 155452 (2009).
[14]A. Iyer, A. Kaskela, L.-S. Johansson, X. Liu, E. I. Kauppinen, and J. Koskinen, "Single walled carbon nanotube network—Tetrahedral amorphous carbon composite film," J. Appl. Phys. **117**, 225302 (2015).
[15]P. N. Nirmalraj, P. E. Lyons, S. De, J. N. Coleman, and J. J. Boland, "Electrical connectivity in single-walled carbon nanotube networks," Nano Lett. **9**, 3890 (2009).
[16]D. M. Larson, K. H. Downing, and R. M. Glaeser, "The surface of evaporated carbon films is an insulating, high-bandgap material," J. Struct. Biol. **174**, 420 (2011).
[17]A. Anders, N. Pasaja, and S. Sansongsiri, "Filtered cathodic arc deposition with ion-species-selective bias," Rev. Sci. Instrum. **78**, 63901 (2007).
[18]A. Anders, I. G. Brown, R. A. MacGill, and M. R. Dickinson, "'Triggerless' triggering of vacuum arcs," J. Phys. D: Appl. Phys. **31**, 584 (1998).
[19]A. Anders and G. Y. Yushkov, "Ion flux from vacuum arc cathode spots in the absence and presence of magnetic fields," J. Appl. Phys. **66**, 4824 (2002).
[20]M. S. Dresselhaus, G. Dresselhaus, R. Saito, and A. Jorio, "Raman spectroscopy of carbon nanotubes," Phys. Rep. **409**, 47 (2005).
[21]J. J. Blackstock, A. A. Rostami, A. M. Nowak, R. L. McCreery, M. R. Freeman, and M. T. McDermott, "Ultraflat carbon film electrodes prepared by electron beam evaporation," Anal. Chem. **76**, 2544 (2004).
[22]A. C. Ferrari and J. Robertson, "Raman spectroscopy of amorphous, nanostructures, diamond-like carbon and nanodiamond," Philos. Trans. R. Soc., A **362**, 2477 (2004).
[23]N. Matsumoto, G. Chen, M. Yumura, D. N. Futaba, and K. Hata, "Quantitative assessment of the effect of purity on the properties of single wall carbon nanotubes," Nanoscale **7**, 5126 (2015).
[24]See supplementary material at http://dx.doi.org/10.1063/1.4948672 for TEM images of coated SWCNTs. Refer to this file for Raman spectra of ta-C coatings used here with D and G peak fits and I(D)/I(G) ratios.
[25]G. U. Sumansekera, C. K. W. Adu, A. Fang, and P. C. Eklund, "Effects of gas adsorption and collisions on electrical transport in single-walled carbon nanotubes," Phys. Rev. Lett. **85**, 1096 (2000).
[26]A. Tchernatinsky, S. Desai, G. U. Sumansekera, C. S. Jayanthi, S. Y. Wu, B. Nagabhirava, and B. Alphenaar, "Adsorption of oxygen molecules on individual single-wall carbon nanotubes," J. Appl. Phys. **99**, 034306 (2006).
[27]W. Ren, A. Iyer, J. Koskinen, A. Kaskela, E. I. Kauppinen, K. Avchaciov, and K. Nordlund, "Conditions for forming composite carbon nanotube-diamond like carbon material that retain the good properties of both materials," J. Appl. Phys. **118**, 194306 (2015).
[28]Y. Lifshitz, S. R. Kasi, J. W. Rabalais, and W. Eckstein, "Subplantation model for film growth from hyperthermal species," Phys. Rev. B **41**, 10468 (1990).
[29]S. Uhlmann, Th. Frauenheim, and Y. Lifshitz, "Molecular-dynamics study of the fundamental processes involved in subplantation of diamond like carbon," Phys. Rev. Lett. **81**, 641 (1998).
[30]C. A. Davis, G. A. J. Amaratunga, and K. M. Knowlws, "Growth mechanism and cross-sectional structure of tetrahedral amorphous carbon thin films," Phys. Rev. Lett. **80**, 3280 (1998).

[31]R. Gaal, J.-P. Salvetat, and L. Forro, "Pressure dependence of the resistivity of single-wall carbon nanotube ropes," Phys. Rev. B **61**, 7320 (2000).
[32]A. Merlen, N. Bendiab, P. Toulemonde, A. Aouizerat, and A. San Miguel, "Resonant Raman spectroscopy of single-wall carbon nanotubes under pressure," Phys. Rev. B **72**, 035409 (2005).
[33]P. V. Teredesai, A. K. Sood, D. V. S. Muthu, R. Sen, A. Govindaraj, and C. N. R. Rao, "Pressure-induced reversible transformation in single-wall carbon nanotube bundles studied by Raman spectroscopy," Chem. Phys. Lett. **319**, 296 (2000).
[34]U. D. Venkateswaran, A. M. Rao, E. Richter, M. Menon, A. Rinzler, R. E. Smalley, and P. C. Eklund, "Probing the single-wall carbon nanotube bundle: Raman scattering under high pressure," Phys. Rev. B **59**, 10928 (1999).
[35]L. Hu, D. S. Hecht, and G. Gruner, "Carbon nanotube thin films: Fabrication, properties and applications," Chem. Rev. **110**, 5790 (2010).
[36]P. M. Ajayan, L. S. Schadler, C. Giannaris, and A. Rubio, "Single-walled carbon nanotube-polymer composites: Strength and weakness," Adv. Mater. **12**, 750 (2000).
[37]Q. Zhao and H. D. Wagner, "Raman spectroscopy of carbon-nanotube-based composite," Philos. Trans. R. Soc., A **362**, 2407 (2004).
[38]S. Anders, D. L. Callahan, G. M. Pharr, T. Y. Tsuic, and C. S. Bhatia, "Multilayers of amorphous carbon prepared by cathodic arc deposition," Surf. Coat. Technol. **94–95**, 189 (1997).
[39]M. Gioti, S. Logothetidis, and C. Charitidis, "Stress relaxation and stability in thick amorphous carbon films deposited in layer structure," Appl. Phys. Lett. **73**, 184 (1998).
[40]D. Sheeja, B. K. Tay, K. W. Leong, and C. H. Lee, "Effect of film thickness on the stress and adhesion of diamond-like carbon coatings," Diamond Relat. Mater. **11**, 1643 (2002).
[41]N. Dwivedi, S. Kumar, S. Singh, and H. K. Malik, "Oxygen modified diamond-like carbon as window layer for amorphous silicon solar cells," Sol. Energy **86**, 220 (2012).